A fully implicit edge/face centered Discontinuous Galerkin / Mixed Finite Element scheme for the Advection-Dispersion Equation

Anis A. Younes, Frederick Delay, Philippe Ackerer

A fully implicit edge/face centered Discontinuous Galerkin / Mixed Finite Element scheme for the Advection-Dispersion Equation

Anis Younes[1], Frederick Delay[1], Philippe Ackerer[1,*]

[1] Institut Terre et Environnement de Strasbourg,

Université de Strasbourg, CNRS, ENGEES, UMR 7063,

5 rue René Descartes

67084 Strasbourg, France

Submitted to Advances in Water Resources

*Contact author: Philippe Ackerer

E-mail: ackerer@unistra.fr

Abstract

Mixed Finite Element (MFE) method is a robust numerical technique for solving elliptic and parabolic partial differential equations (PDEs). However, MFE can generate solutions with strong unphysical oscillations and/or large numerical diffusion for hyperbolic type PDEs. For its part, Discontinuous Galerkin (DG) finite element method is well adapted to solve hyperbolic systems and can accurately reproduce solutions involving sharp fronts. Therefore, the combination of DG and MFE is a good strategy for solving hyperbolic/parabolic problems such as advection – diffusion/dispersion equations. The classical formulation of the two methods is based on operator and time splitting allowing for separate solutions to advection with an explicit scheme and to dispersion with an implicit scheme. However, this kind of approach has the following drawbacks: (*i*) it lacks efficiency, as two systems with different unknowns are solved at each time step, (*ii*) it induces errors generated by the splitting, (*iii*) it can be CPU wise-expensive because of the CFL constraint, and (*iv*) it cannot be employed for steady-state transport simulations.

To overcome these difficulties, we develop in this work a fully implicit edge/face centered DG-MFE formulation where the two methods share the same unknowns. In this formulation, the DG method is developed on lumping regions associated with the mesh edges/faces instead of mesh elements. Thus, the traces of concentration at mesh edges/faces, which are the Degrees Of Freedom (DOF) of the hybrid-MFE, are also part of the DOFs of the DG. The temporal discretization is based on the Crank–Nicolson method for both advection and dispersion. Numerical tests are performed to validate the new scheme by comparison against an analytical solution and to show its ability to handle steady-state transport simulations.

The procedure is developed for 2D triangular meshes but can easily be extended to other 2D and 3D shape elements.

Keywords:

Advection dispersion, transport, Mixed Finite Element, Discontinuous Galerkin, numerical oscillations.

Highlights

- Advection-dispersion solved at once by mixed and discontinuous finite elements.
- Comparisons with analytical solutions show the accuracy of the new scheme.
- Numerical tests show its ability to use large time steps and to achieve steady-state simulations.

1. Introduction

Numerous physical processes are described by mathematical models using partial differential equations (PDEs) of elliptic or parabolic types (as for instance, steady-state diffusion or transient energy conduction) or of hyperbolic type (advection, shock propagation). Nowadays, many numerical methods exist to solve these PDEs, mainly based on finite volume or finite element approaches. We will focus here on the solution of the advection-dispersion equation (ADE) governing solute transport in porous media. Compared to diffusion, dispersion is an anisotropic process, described by a full tensor which depends on the fluid velocity, contrarily to diffusion, described by a scalar coefficient independent of the velocity. Therefore, according to the velocity distribution and magnitude, the transport process can locally be either advection or dispersion dominated. Moreover, the dispersion tensor is a full tensor which is discontinuous over space. To address these challenges, mixed and discontinuous finite element methods have become more and more popular over the last decades.

Mixed Finite Element (MFE) ([1], [2], [3]) is a robust numerical method, well adapted to solving elliptic and parabolic diffusion problems such as fluid flow or diffusion transport equations in porous media. The MFE method is locally conservative; it rigorously treats highly heterogeneous domains with full permeability and dispersion tensors and can easily handle unstructured meshes ([4]). MFE provides more accurate fluxes than conventional numerical methods ([5], [6]) and is more accurate than Local Discontinuous Galerkin (LDG) method for non-smooth grids ([7]). The hybridization technique, initially proposed by [8], allows for reducing the number of unknowns of the original MFE and results in a final system with a symmetric positive-definite matrix ([9], [10]). The unknowns with the hybrid-MFE method are the traces (also seen as average values) of the scalar variable at mesh edges (2D) or faces (3D) ([2]). A lumped formulation of the MFE method has been developed in [11] to improve its monotonicity and reduce the unphysical over- and under-shoots observed when simulations of

diffusion with small time steps are performed ([12], [13]). When the classical MFE method is employed for advection diffusion transport, it returns solution with spurious oscillations because of the hyperbolic nature of the advection equation ([14], [15]). The combination of MFE with an upwind scheme renders a stable solution but with excessive numerical diffusion smearing the sharp concentration front in the case of advection dominated transport ([15]).

Discontinuous Galerkin finite element (DG) method is well adapted to hyperbolic problems ([14]). The method has been developed for hyperbolic ([16], [17], [18]) and elliptic equations ([19], [20], [21]). However, contrarily to DG applied to elliptic equations, the DG applied to hyperbolic systems is clearly more accurate than other existing finite element methods ([22]). The DG method yields a high-resolution scheme which is strictly conservative at the element level and can accurately solve problems involving sharp front propagations ([14]). When used with an explicit scheme, the time-step size has to fulfil the Courant–Friedrichs–Levy (CFL) condition and a slope-limiting procedure is necessary to ensure the stability of the solution ([23], [24], [25]). The DG method can also be used with an implicit time discretization which avoids both the CFL constraint and the slope limiting procedure ([26]). In the literature, DG is often used with piecewise linear approximation and with degrees of freedom (DOF) corresponding to the discontinuous interior concentrations at the nodes of each element (see, for example, [2], [14], [27], [28]).

Both mixed and discontinuous finite element methods have the interesting property of preserving mass locally, and as such, they can be linked to the finite volume method. For instance, the MFE method was shown to be equivalent to some finite volume methods in ([29], [30],[31]). For its part, the DG method is a high-resolution scheme for advection that maintains the local conservation of finite volume methods but also allows for high-order approximations through a variational formulation instead of a functional reconstruction [32].

Thus, an efficient way to solve the ADE is to rely upon the most appropriate method for each operator, that is, MFE for the diffusion operator and DG for advection. However, because MFE and DG methods use different DOFs, their combination requires additional approximations. In the literature, the combination has been ensured by operator and time splitting ([14], [27], [28], [33], [34]), a procedure which is based on the following two steps (see [14] for details):

1. the advection equation is solved with the DG method to obtain the concentrations at the new time level.
2. these concentrations are used as initial concentrations to solve the dispersion equation with the MFE method.

The time splitting procedure has been employed in [35], [36] and [37] by coupling the implicit MFE method in its hybrid form for dispersion with high resolution explicit finite volumes for advection. In [38], it is suggested to use the linear Galerkin method instead of the MFE method for the dispersion operator in the case of strong anisotropic dispersion tensor coefficients.

Note that one of the major drawbacks of the explicit time discretization of advection is a time step selection based on the CFL condition which requires the time step to be less than the time for flow to pass through one mesh element. The impact of this condition can be highly severe in the case of local mesh refinement and/or locally high velocity magnitude such as around injection or pumping wells. To alleviate this drawback, spatially variable time stepping procedures have been developed to improve computational efficiency (e.g., [39, 40]), but their usage remains scarce due to the difficulty of their implementation when the velocity field changes at each time step.

To sum up, the classical MFE-DG combination based on operator and time splitting procedure is convenient but has the following drawbacks: (*i*) the procedure is not very efficient since two linear systems with different unknowns are solved at each time step, (*ii*) the procedure generates splitting errors which can be important for large time steps, (*iii*) it can be CPU-wise expensive

in the case of explicit time discretization of advection, and (*iv*) steady-state transport simulations cannot be performed.

The main objective of this work is to develop a new and alternative coupling of the MFE and DG methods that avoids these drawbacks. The basic idea in this formulation is to develop the DG method on the lumping regions associated with the mesh edges/faces, instead of mesh elements. In this way, the traces of concentration at mesh edges/faces, which are the DOFs of the hybrid-MFE, are also part of the DOFs of the DG. This yields a unique system where advection and dispersion are assembled and solved simultaneously. In this way, the proposed scheme uses different numerical techniques that are specifically suited to achieve high accuracy for each type of equation while avoiding the splitting procedure. Both advection and dispersion are discretized with the Crank-Nicolson implicit time discretization which allows for both large time steps and steady-state transport simulation in a single step.

The outline of the paper is as follows. Section 2, reminds us on the classical approach combining MFE and DGs based on operator and time splitting. In Section 3, we present the lumped-MFE for the discretization of the dispersive transport equation. In Section 4, we introduce the edge/face centred DG method for advection and its combination with the lumped-MFE for dispersion. Numerical experiments are reported in the last Section to investigate on the efficiency and accuracy of the new approach for advection-dispersion problems.

2. The classical MFE-DG formulation for the advection-dispersion equation

In this section, we recall the main steps of the classical MFE-DG formulation to solve the advection-dispersion equation, based on the operator and time splitting procedure.

2.1 The advection-dispersion transport equation

The transport of a non-reactive solute in a saturated porous medium is governed by the following advection-dispersion equation:

$$\varepsilon \frac{\partial C}{\partial t} + \nabla.\left(\boldsymbol{q}_a + \boldsymbol{q}_d\right) = 0 \tag{1}$$

where C is the concentration [ML^{-3}], ε is the porosity [L^3L^{-3}],], t is the time [T], $\boldsymbol{q}_a = \boldsymbol{q}C$ is the advective flux with $\boldsymbol{q}$ the Darcy velocity [LT^{-1}], and $\boldsymbol{q}_d$ is the dispersive flux given by:

$$\boldsymbol{q}_d = -\boldsymbol{D}\nabla C \tag{2}$$

with $\boldsymbol{D}$, the dispersion tensor, expressed by:

$$\boldsymbol{D} = D_m \boldsymbol{I} + \left(\alpha_L - \alpha_T\right)\boldsymbol{q} \otimes \boldsymbol{q} / \left|\boldsymbol{q}\right| + \alpha_T \left|\boldsymbol{q}\right| \boldsymbol{I} \tag{3}$$

in which α_L and α_T are the longitudinal and transverse dispersivities [L]. D_m is the pore water diffusion coefficient [L^2T^{-1}] and $\boldsymbol{I}$ is the unit (diagonal) tensor.

Equation (1) is subject to the following initial and boundary conditions:

$$\begin{aligned}
&C\left(\boldsymbol{x},0\right) = C_0\left(\boldsymbol{x}\right) && \boldsymbol{x} \in \Omega \\
&C\left(\boldsymbol{x},t\right) = g_1\left(\boldsymbol{x},t\right) && \left(\boldsymbol{x} \in \partial\Omega^1, t > 0\right) \\
&\left(\boldsymbol{q}C - \boldsymbol{D}\nabla C\right).\boldsymbol{\eta}_{\partial\Omega} = g_2\left(\boldsymbol{x},t\right) && \left(\boldsymbol{x} \in \partial\Omega^2, t > 0\right) \\
&\left(-\boldsymbol{D}\nabla C\right).\boldsymbol{\eta}_{\partial\Omega} = 0 && \left(\boldsymbol{x} \in \partial\Omega^3, t > 0\right)
\end{aligned} \tag{4}$$

where Ω is a bounded, polygonal open set of R^2, $\partial\Omega^1$, $\partial\Omega^2$ and $\partial\Omega^3$ are partitions of the boundary $\partial\Omega$ of Ω corresponding to Dirichlet, total flux, and outflow boundary conditions, respectively and $\boldsymbol{\eta}_{\partial\Omega}$ is the unit outward normal to the boundary $\partial\Omega$. The outflow boundary condition considered in this work corresponds to a null dispersive flux (*i.e.*, the solute exits only by advection).

2.2 The operator and time splitting procedure

Operator and time splitting (e.g., [33]) offers the possibility to adapt the numerical technique to each type of PDE. To this aim, the advection equation is solved first by writing:

179 $$\varepsilon \frac{C^{n+1,ad} - C^{n}}{\Delta t} + \nabla . \left(\boldsymbol{q}_a \right) = 0 \quad (5)$$

180 where C^n is the known concentration at the previous time level $\left(n\right)$ and $C^{n+1,ad}$ is the
181 concentration at the new time level $\left(n+1\right)$ due to the advection process only.

182 In a second step, the dispersion equation is solved using $C^{n+1,ad}$ as the initial concentration:

183 $$\varepsilon \frac{C^{n+1} - C^{n+1,ad}}{\Delta t} + \nabla . \left(\boldsymbol{q}_d \right) = 0 \quad (6)$$

184 where C^{n+1} is the final concentration at the new time level $\left(n+1\right)$ resulting from both advection
185 and dispersion.

186

187 ***2.3 The DG discretization of the advection part of the transport equation***

188 The advection equation (5) solved by DG is usually approximated by linear functions (P1-DG)
189 on triangles:

190 $$C_E\left(x,y\right) = \sum_{i=1}^{3} \phi_E^i C_E^i \quad (7)$$

191 where $C_E^i \left(i = 1,..,3\right)$ are the three DOFs for the approximated concentration.

192 The DOFs of the P1-DG generally correspond to the discontinuous concentrations at the nodes
193 ([2], [7], [27], [28]). Thus, C_E^i is the concentration at the node i of element E and ϕ_E^i is the
194 classical linear chapeau interpolation function (see Fig. 1).

195

196

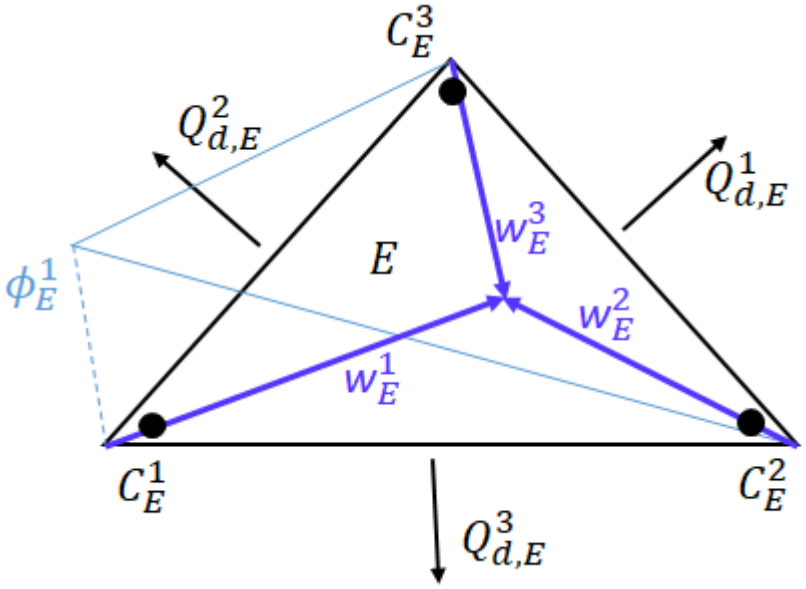

197

198 **Fig. 1.** DOFs (C_E^i) for the classical P1-DG, linear chapeau interpolation function (ϕ_E^i),

199 Raviart-Thomas vector basis functions (w_E^j), and diffusive fluxes ($Q_{d,E}^i$) through the edges of

200 an element E.

201 Assuming a constant porosity over the element, the variational formulation of Eq. (5) on the

202 element E using the test function ϕ_E^i writes:

203 $$\varepsilon_E \sum_j \frac{dC_E^j}{dt} \int_E \phi_E^j \phi_E^i dx + \int_E \nabla.\left(\boldsymbol{q} C \phi_E^i\right) dx - \sum_j \int_E C_E^j \phi_E^j \, \boldsymbol{q}.\nabla \phi_E^i dx = 0 \quad (8)$$

204 By approximating the Darcy velocity $\boldsymbol{q}$ inside each triangular element E with the lowest order

205 Raviart-Thomas (RT0) basis functions, the second term of Eq. (8) can be transformed into a

206 boundary element integral and evaluated using upstream concentrations as:

207 $$\int_E \nabla.\left(\boldsymbol{q} C \phi_E^i\right) dx = \sum_{j=1}^{3} \frac{Q_E^j}{\left|\partial E_j\right|} \int_{\partial E_j} \overline{C}_{E*}^j \phi_E^i d\gamma \quad (9)$$

208 where $\overline{C}_{E*}^j$ is the upstream concentration at the edge ∂E_j of element E. It is either calculated

209 as the approximation of the concentration in the element E in the case of outflow

210 $\left(\overline{C}_{E*}^j = \overline{C}_E^j \ if \ Q_E^j > 0\right)$, or the approximated concentration of its adjacent element E' in the case

of inflow $\left(\overline{C}^j_{E*} = \overline{C}^j_{E'} \text{ if } Q^j_E < 0\right)$. $Q^j_E = \int_{\partial E_j} \boldsymbol{q}.\boldsymbol{\eta}_{\partial E_j} d\gamma$ is the water flux (counted positive for outflow) across the edge ∂E_j of unit outward normal vector $\boldsymbol{\eta}_{\partial E_j}$ and shared by the two adjacent elements E and E'.

Substituting Eq. (9) into Eq. (8) and using the three test functions ϕ^i_E leads to a local system of ordinary differential equations for the DOFs of element E and eventually for the DOFs of its three adjacent elements. In the case of an explicit time discretization, this local system is independently solved for each element E to obtain $C^{i,adv}_E$, the concentrations at the node $i = 1,..,3$ of the element E at the new time level. In the case of an implicit or a θ-scheme temporal discretization, all local systems are assembled into a global system, then solved to obtain all the $C^{i,adv}_E$ of all elements. Then, the mean concentration at each element E due to advection is calculated as the average of the three nodal concentrations $\left(C^{adv}_E = \frac{1}{3}\sum_{i=1}^{3} C^{i,adv}_E\right)$ and used as a starting concentration for the solution of the dispersion equation.

2.4 The MFE discretization of the dispersion equation

The dispersive flux $\boldsymbol{q}_d$ is approximated using the Raviart-Thomas (RT0) vectorial basis functions $\boldsymbol{w}^j_E$:

$$\boldsymbol{q}_d = \sum_{j=1}^{3} Q^j_{d,E} \boldsymbol{w}^j_E \tag{10}$$

where $Q_{d,E}^{j} = \int_{j} \boldsymbol{q}_d . \boldsymbol{\eta}_j^E d\gamma$ is the dispersive flux across the edge ∂E_j of element E and

$\boldsymbol{w}_E^j = \frac{1}{2|E|}\begin{pmatrix} x - x_E^j \\ y - y_E^j \end{pmatrix}$ is the RT0 basis function ([4]), with $\left(x_E^j, y_E^j\right)$ the coordinates of the node

j opposite to the edge ∂E_j of E and $|E|$ the area of E (see Fig. 1).

The variational formulation of Eq. (2) (rewritten as $\nabla C = -\boldsymbol{D}^{-1}\boldsymbol{q}$) over the element E using

the test function $\boldsymbol{w}_E^i$ yields:

$$\int_E \boldsymbol{D}_E^{-1}\boldsymbol{q}_d \boldsymbol{w}_E^i dx = \int_E C\nabla . \boldsymbol{w}_E^i dx - \sum_j \int_{\partial E_j} C\boldsymbol{w}_E^i . \boldsymbol{\eta}_E^j d\gamma \tag{11}$$

where $\boldsymbol{D}_E$ is the local dispersion tensor at the element E and $\boldsymbol{\eta}_E^j$ the unit outward normal vector

to the edge ∂E_j.

Using Eq. (10) and properties of $\boldsymbol{w}_E^i$ (see [4] for details) results in:

$$\sum_j Q_{d,E}^j \int_E \left(\boldsymbol{D}_E^{-1}\boldsymbol{w}_E^j\right).\boldsymbol{w}_E^i dx = C_E - TC_E^i \tag{12}$$

where C_E is the mean concentration at element E and TC_E^i is the mean concentration at the

edge ∂E_i. Inverting Eq. (12) yields the following expression for the dispersive flux $Q_{d,E}^i$:

$$Q_{d,E}^i = \sum_j B_{i,j}^{E,-1}\left(C_E - TC_E^j\right) \tag{13}$$

where $B_{i,j}^E = \int_E \left(\boldsymbol{D}_E^{-1}\boldsymbol{w}_E^j\right).\boldsymbol{w}_E^i dx$ are the terms of a local matrix $\boldsymbol{B}^E$, assuming that the tensor $\boldsymbol{D}_E$

is constant over the element E.

The MFE solution of the dispersion Eq. (6) is then calculated in two steps as follows:

Step1: A finite volume (FV) discretization of the dispersion equation over the element E is

written using an implicit scheme and starting with C_E^{adv}:

$$\varepsilon_E \frac{|E|}{\Delta t}\left(C_E^{\,n+1} - C_E^{adv}\right) + \sum_i Q_{d,E}^{i,n+1} = 0 \tag{14}$$

Substituting Eq. (13) into Eq. (14) gives C_E^{n+1} as:

$$C_E^{n+1} = \frac{1}{\beta_E} \sum_i \alpha_E^i TC_E^{i,n+1} + \frac{\lambda_E}{\beta_E} C_E^{adv} \tag{15}$$

in which $\alpha_E^i = \sum_j B_{i,j}^{E,-1}$, $\alpha_E = \sum_i \alpha_E^i$, $\lambda_E = \varepsilon_E \frac{|E|}{\Delta t}$ and $\beta_E = \lambda_E + \alpha_E$.

Finally, plugging Eq. (15) with the dispersive flux Eq. (13) yields:

$$Q_{d,E}^{i,n+1} = \sum_j \left(\frac{\alpha_E^i \alpha_E^j}{\beta_E} - B_{i,j}^{E,-1} \right) TC_E^{j,n+1} + \frac{\lambda_E}{\beta_E} \alpha_E^i C_E^{adv} \tag{16}$$

Step2: At each interior edge ∂E_i, shared by the two adjacent elements E and E', the continuity of the dispersive flux is written as:

$$Q_{d,E}^{i,n+1} + Q_{d,E'}^{i,n+1} = 0 \tag{17}$$

Thus, substituting Eq. (16) into Eq. (17) renders the final system solved to obtain the traces of concentration at edges $TC_E^{i,n+1}$ at the new time level.

Knowing the values $TC_E^{i,n+1}$, the average concentration at the new time level C_E^{n+1} can be calculated using Eq. (15) and the nodal concentrations (the DOFs of DG) are updated by equally distributing the change of mass due to dispersion in the element E:

$$C_E^{i,n+1} = C_E^{i,n} + \left(C_E^{n+1} - C_E^{adv} \right) \tag{18}$$

These nodal concentrations are then used as initial DG concentrations for the new time step calculation solving Eq. (8).

3. The new edge-centered MFE-DG formulation

The previous classical MFE-DG formulation suffers from loss of efficiency. In the case of implicit time discretization, two different systems must be solved at each time step, generating

significant splitting errors in the case of large time steps ([30]). In addition, the scheme cannot treat steady-state transport simulations. To overcome these difficulties, we present in this section a new MFE-DG formulation where the two methods are developed with the same DOFs on mesh edges. We rely upon the lumped formulation developed by [11] for the MFE method, to which we combine the DG method developed on the lumping regions associated with the mesh edges.

3.1 The lumped hybrid-MFE method for dispersion transport

We consider a simplex region S_E^i, associated with each edge ∂E_i of an element E by joining the centre of *E* with the nodes *j* and *k* forming the edge i (Fig. 2). A lumping region R_i (the grey area in Fig. 2), is then associated with the edge i. It is formed by the two simplex regions S_E^i and $S_{E'}^i$ for an interior edge i, shared by two adjacent elements E and E'. For a boundary edge i, the lumping region R_i is only formed by the single simplex region S_E^i.

The lumped MFE formulation is developed in two steps as follows ([15]):

Step1: The transient term is not considered, resulting in a dispersive transport over the element *E* written as:

$$\sum_i \underline{Q}_{d,E}^{i,n+1} = 0 \tag{19}$$

with $\underline{Q}_{d,E}^{i,n+1}$ the steady-state dispersive fluxes across the edges i.

Using Eq. (13), we obtain:

$$C_E^{n+1} = \sum_i \frac{\alpha_E^i}{\alpha_E} TC_E^{i,n+1} \tag{20}$$

and Eq. (16) reduces to:

$$\underline{Q}_{d,E}^{i,n+1} = \sum_j \left(\frac{\alpha_E^i \alpha_E^j}{\alpha_E} - B_{i,j}^{E,-1} \right) TC_E^{j,n+1} \tag{21}$$

Step2: The transient term is allocated to the mesh edges and not to the element by simply writing the FV dispersion equation over the lumping region R_i:

$$\int_{R_i} \varepsilon \frac{\partial C}{\partial t} dx + \int_{R_i} \nabla . \boldsymbol{q}_d dx = 0 \tag{22}$$

where R_i is associated with the edge i corresponding to ∂E_i of concentration TC_E^i. This leads to (see notations in Fig. 2):

$$\left(\varepsilon_E \frac{|E|}{3} + \varepsilon_{E'} \frac{|E'|}{3} \right) \frac{\partial TC_E^i}{\partial t} + \underline{Q}_{d,E}^{ij,n+1} + \underline{Q}_{d,E}^{ik,n+1} + \underline{Q}_{d,E'}^{ij,n+1} + \underline{Q}_{d,E'}^{ik,n+1} = 0 \tag{23}$$

where $\underline{Q}_{d,E}^{i\alpha,n+1}$ are the (interior) dispersive fluxes through the edges of R_i. Using Eq. (10), an interior dispersive flux between the lumping regions R_i and R_j writes:

$$\underline{Q}_{d,E}^{ij,n+1} = \frac{1}{3} \left(\underline{Q}_{d,E}^{j,n+1} - \underline{Q}_{d,E}^{i,n+1} \right) \tag{24}$$

Hence, Eq.(23) becomes:

$$\left(\varepsilon_E \frac{|E|}{3} + \varepsilon_{E'} \frac{|E'|}{3} \right) \frac{\partial TC_E^i}{\partial t} - \underline{Q}_{d,E}^{i,n+1} - \underline{Q}_{d,E'}^{i,n+1} = 0 \tag{25}$$

Substituting Eq. (21) in Eq. (25), we obtain the final system to solve for dispersive transport in the form:

$$\left(\varepsilon_E \frac{|E|}{3} + \varepsilon_{E'} \frac{|E'|}{3} \right) \frac{\partial TC_E^i}{\partial t} + \sum_j \left(B_{i,j}^{E,-1} - \frac{\alpha_E^i \alpha_E^j}{\alpha_E} \right) TC_E^{j,n+1} + \sum_j \left(B_{i,j}^{E',-1} - \frac{\alpha_{E'}^i \alpha_{E'}^j}{\alpha_{E'}} \right) TC_{E'}^{j,n+1} = 0 \tag{26}$$

It is worth noting that the solution of this system has an improved monotonicity compared to the standard hybrid MFE formulation (see [11]). Indeed, with the lumped formulation, the maximum principle is respected for parabolic diffusion equations on acute triangulations, which is not the case of the standard mixed hybrid finite element method. For more general shapes of 2D and 3D elements, numerical experiments showed that the lumping procedure significantly improved the monotonous character of the hybrid-MFE solution [11]. The lumped formulation

was applied to unsaturated flow and revealed more efficient and more robust than the standard hybrid formulation for both unfractured ([41]) and fractured ([42]) aquifers.

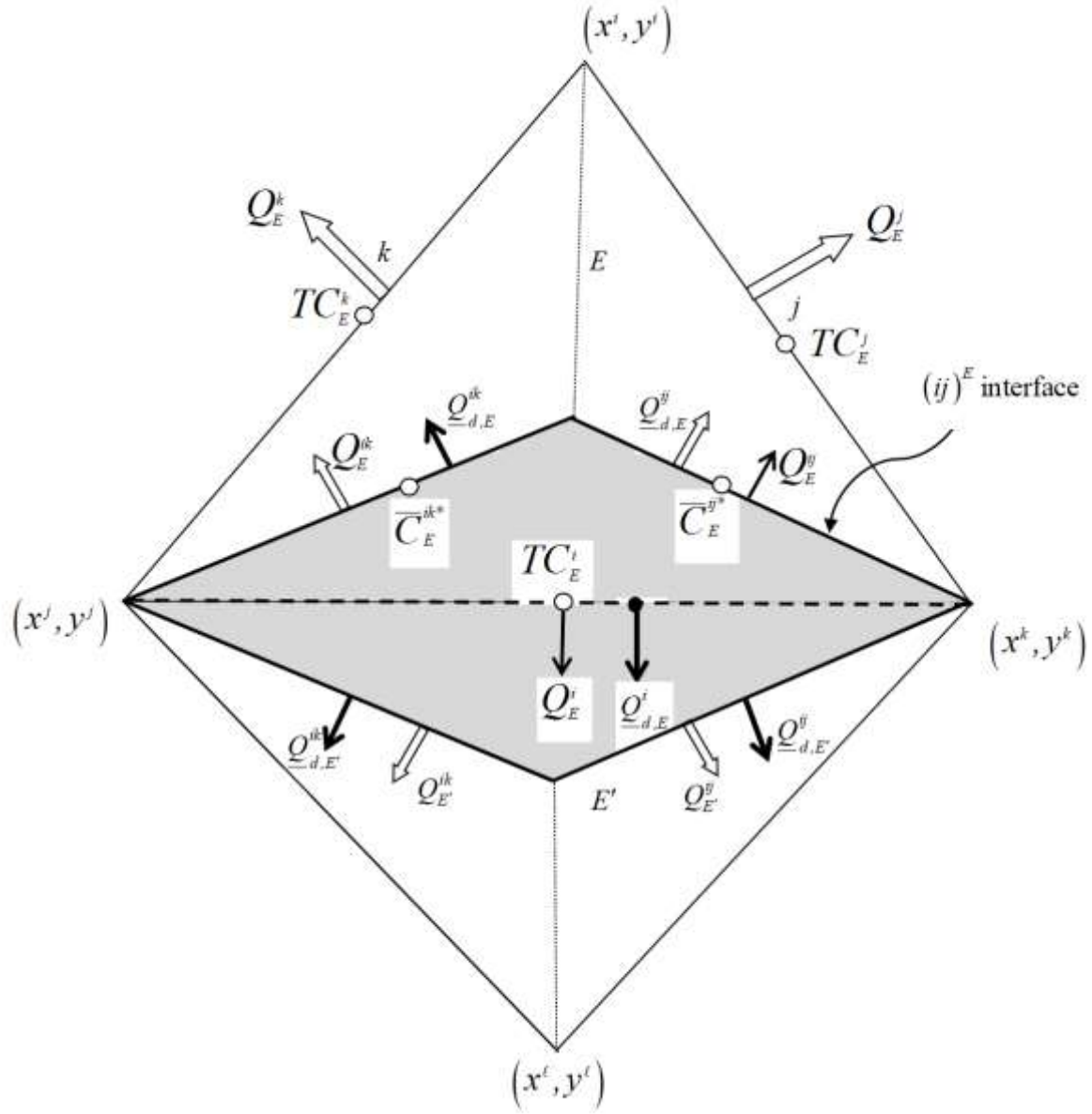

Fig. 2: The lumping region R_i associated with the edge ∂E_i, sharing the elements E and E' and formed by the two simplex regions S_E^i and $S_{E'}^i$.

317 *3.2 The edge/face centred DG-MFE scheme for advection dispersion transport*

318 The main idea of the new scheme is to combine an edge-based upwind DG method for advection
319 with the previously discussed lumped hybrid-MFE for dispersion. The DG method is developed
320 on the dual mesh formed by the lumping regions R_i instead of the original mesh formed by the
321 elements E.

322 The concentration over each lumping region R_i is approximated via linear basis
323 functions ϕ_i^m as:

324 $$C_i(\boldsymbol{x},t) = \sum_{m=1}^{3} \tilde{C} \qquad \boldsymbol{x}) \tag{27}$$

325 where $\tilde{C}$ are the new DOFs for the P1-DG concentration approximation.

326 For each lumping region R_i centred at $(\bar{x}_i, \bar{y}_i)$, the new DOFs correspond to the edge
327 concentration TC^i considered as the mean concentration at R_i, associated with a deviation of
328 the concentration in each space direction ([18]) evaluated by the three following interpolation
329 functions:

330 $$\begin{aligned} &\tilde{C} \qquad ^{i}, && \phi_i^1(x,y) = 1 \\ &\tilde{C} \qquad \frac{\bar{x}_i}{\partial x}, && \phi_i^2(x,y) = x - \bar{x}_i, \\ &\tilde{C} \qquad \frac{\bar{y}_i}{\partial y}, && \phi_i^3(x,y) = y - \bar{y}_i. \end{aligned} \tag{28}$$

331 The variational formulation of the whole transport equation (1) over the lumping area R_i using
332 ϕ_i^m as test functions writes:

333 $$\int_{R_i} \varepsilon \frac{\partial C_i}{\partial t} \phi_i^m dx + \int_{R_i} \nabla.(\boldsymbol{q} C_i) \phi_i^m k dx + \int_{R_i} (\nabla.\boldsymbol{q}_d) \phi_i^m dx = 0 \tag{29}$$

334 The first integral corresponds to the (mass) accumulation term:

335 $$\int_{R_i} \varepsilon \frac{\partial C_i}{\partial t} \phi_i^m dx = \sum_{l=1}^{3} \frac{\partial \tilde{C}}{\partial t} \int_{R_i} \varepsilon \psi_l \psi_i \, dx \tag{30}$$

Using Green's formula, the second integral in Eq. (29) is decomposed into:

$$\int_{R_i} \nabla.\left(\boldsymbol{q}C_i\right)\phi_i^m dx = \int_{\partial R_i} C^*\phi_i^m \boldsymbol{q}.\boldsymbol{\eta}_{\partial R_i} d\gamma - \sum_{l=1}^{3} \tilde{C} \qquad \phi_i^m dx \tag{31}$$

in which, the boundary integral is developed as (see notations in Fig. 2):

$$\int_{\partial R_i} C^*\phi_i^m \boldsymbol{q}.\boldsymbol{\eta}_{\partial R_i} d\gamma = \frac{Q_E^{ij}}{\left|E_{ij}\right|}\int_{E_{ij}} \overline{C}_E^{ij*}\phi_i^m d\gamma + \frac{Q_E^{ik}}{\left|E_{ik}\right|}\int_{E_{ik}} \overline{C}_E^{ik*}\phi_i^m d\gamma + \frac{Q_{E'}^{ik}}{\left|E'_{ik}\right|}\int_{E'_{ik}} \overline{C}_{E'}^{ik*}\phi_i^m d\gamma + \frac{Q_{E'}^{ij}}{\left|E'_{ij}\right|}\int_{E'_{ij}} \overline{C}_{E'}^{ij*}\phi_i^m d\gamma \tag{32}$$

where Q_E^{ij} is the water flux across the interior interface E_{ij} (between R_i and R_j) of length $\left|E_{ij}\right|$. $\overline{C}_E^{ij*}$ is the upstream concentration at E_{ij}, defined as:

$$\overline{C}_E^{ij*} = \lambda_i^{E,ij}\overline{C}_i^{ij} + \left(1-\lambda_i^{E,ij}\right)\overline{C}_j^{ij} \tag{33}$$

where $\overline{C}_i^{ij}$ (respectively $\overline{C}_j^{ij}$) is the concentration at the interface E_{ij} calculated by the approximation (Eq. (27)) of the concentration in R_i (respectively R_j) and $\lambda_i^{E,ij}$ is defined at E_{ij} by:

$$\lambda_i^{E,ij} = \begin{cases} 1 & if \quad Q_E^{ij} \geq 0 \\ 0 & if \quad Q_E^{ij} < 0 \end{cases} \tag{34}$$

The third term in Eq. (29) corresponds to the dispersion integral, which is approximated by:

$$\int_{R_i} \left(\nabla.\boldsymbol{q}_d\right)\phi_i^m dx = \frac{1}{\left|R_i\right|}\left(\underline{Q}_{d,E}^{ij,n+1} + \underline{Q}_{d,E}^{ik,n+1} + \underline{Q}_{d,E'}^{ij,n+1} + \underline{Q}_{d,E'}^{ik,n+1}\right)\int_{R_i} \phi_i^m dx \tag{35}$$

Using Eq. (24) in Eq. (35) renders:

$$\int_{R_i} \left(\nabla.\boldsymbol{q}_d\right)\phi_i^m dx = -\frac{1}{\left|R_i\right|}\left(\underline{Q}_{d,E}^{i,n+1} + \underline{Q}_{d,E'}^{i,n+1}\right)\int_{R_i} \phi_i^m dx \tag{36}$$

Substituting Eq. (21) in Eq. (36) results in:

$$\int_{R_i} \left(\nabla.\boldsymbol{q}_d\right)\phi_i^m dx = -\frac{1}{\left|R_i\right|}\left(\sum_l \left(\frac{\alpha_E^i\alpha_E^l}{\alpha_E} - B_{i,l}^{E,-1}\right)TC_E^{l,n+1} + \sum_l \left(\frac{\alpha_{E'}^i\alpha_{E'}^l}{\alpha_{E'}} - B_{i,l}^{E',-1}\right)TC_{E'}^{l,n+1}\right)\int_{R_i} \phi_i^m dx \tag{37}$$

354 Hence, using the three test functions ϕ_i^m in Eq. (29) leads to the following local system:

$$
\left[A\right]\begin{bmatrix} \dfrac{\partial \tilde{C}}{\partial t} \\ \dfrac{\partial \tilde{C}}{\partial t} \\ \dfrac{\partial \tilde{C}}{\partial t} \end{bmatrix} = \left[B\right]\begin{bmatrix} \tilde{C} & \tilde{C} & \tilde{C} \\ \tilde{C} & \tilde{C} & \tilde{C} \\ \tilde{C} & \tilde{C} & \tilde{C} \end{bmatrix}_E
$$

355 $$
-\left[M^3+N^3\right]\begin{bmatrix} \tilde{C} \\ \tilde{C} \\ \tilde{C} \end{bmatrix}_{E'} - \left[M^4+N^4\right]\begin{bmatrix} \tilde{C} & & \\ \tilde{C} & & \\ \tilde{C} & & \end{bmatrix}_E \qquad (38)
$$

356 with

$$
A_{l,m} = \int_{R_i} \varepsilon \phi_i^l \phi_i^m dx, \qquad B_{l,m} = \int_{R_i} \phi_i^l \boldsymbol{q}.\nabla \phi_i^m dx
$$

$$
M_{l,m}^0 = \lambda_i^{E,ij} \frac{Q_E^{ij}}{\left|E_{ij}\right|} \int_{E_{ij}} \phi_i^l \phi_i^m d\gamma + \lambda_i^{E,ik} \frac{Q_E^{ik}}{\left|E_{ik}\right|} \int_{E_{ik}} \phi_i^l \phi_i^m d\gamma + \lambda_i^{E',ij} \frac{Q_{E'}^{ij}}{\left|E'_{ij}\right|} \int_{E'_{ij}} \phi_i^l \phi_i^m d\gamma + \lambda_i^{E',ik} \frac{Q_{E'}^{ik}}{\left|E'_{ik}\right|} \int_{E'_{ik}} \phi_i^l \phi_i^m d\gamma
$$

$$
N_{l,m}^0 = \left(\frac{\alpha_E^i \alpha_E^i}{\alpha_E} - B_{i,i}^{E,-1}\right)\delta_{1,l}\delta_{1,m} + \left(\frac{\alpha_{E'}^i \alpha_{E'}^i}{\alpha_{E'}} - B_{i,i}^{E',-1}\right)\delta_{1,l}\delta_{1,m}
$$

$$
M_{l,m}^1 = \left(1-\lambda_i^{E,ij}\right)\frac{Q_E^{ij}}{\left|E_{ij}\right|} \int_{E_{ij}} \phi_j^l \phi_i^m d\gamma, \qquad N_{l,m}^1 = \left(\frac{\alpha_E^i \alpha_E^j}{\alpha_E} - B_{i,j}^{E,-1}\right)\delta_{1,l}\delta_{1,m}
$$

$$
M_{l,m}^2 = \left(1-\lambda_i^{E,ik}\right)\frac{Q_E^{ik}}{\left|E_{ik}\right|} \int_{E_{ik}} \phi_k^l \phi_i^m d\gamma, \qquad N_{l,m}^2 = \left(\frac{\alpha_E^i \alpha_E^k}{\alpha_E} - B_{i,k}^{E,-1}\right)\delta_{1,l}\delta_{1,m}
$$

$$
M_{l,m}^3 = \left(1-\lambda_i^{E',ij}\right)\frac{Q_{E'}^{ij}}{\left|E'_{ij}\right|} \int_{E'_{ij}} \phi_j^l \phi_i^m d\gamma, \qquad N_{l,m}^3 = \left(\frac{\alpha_{E'}^i \alpha_{E'}^j}{\alpha_{E'}} - B_{i,j}^{E',-1}\right)\delta_{1,l}\delta_{1,m}
$$

357 $$
M_{l,m}^4 = \left(1-\lambda_i^{E',ik}\right)\frac{Q_{E'}^{ik}}{\left|E'_{ik}\right|} \int_{E'_{ik}} \phi_k^l \phi_i^m d\gamma, \qquad N_{l,m}^4 = \left(\frac{\alpha_{E'}^i \alpha_{E'}^k}{\alpha_{E'}} - B_{i,k}^{E',-1}\right)\delta_{1,l}\delta_{1,m}
$$

358 If the edge ∂E_j of element E is a boundary edge with a prescribed concentration

359 $\overline{TC_j} = g_1(\mathrm{x},t)$, the term $\left[M^1+N^1\right]\begin{bmatrix} \tilde{C} \\ \tilde{C} \\ \tilde{C} \end{bmatrix}$, in Eq. (38) is replaced by

360 $\left(\left(1-\lambda_i^{E,ij}\right)Q_E^{ij}+\left(\frac{\alpha_E^i\alpha_E^j}{\alpha_E}-B_{i,j}^{E,-1}\right)\right)\begin{pmatrix} g_1 \\ 0 \\ 0 \end{pmatrix}$ and placed in the right hand side of the system to solve.

361 If ∂E_i is a boundary edge with a total flux $Q_t^i = g_2(\boldsymbol{x},t)$, all the contributions of the element
362 E' are removed from Eq. (38). Finally, if the edge ∂E_i is an outflow boundary with a null
363 diffusive flux, the total flux Q_t^i in the system (38) is replaced by the advective flux $Q_E^i\tilde{c}$.
364 The time discretization of the system (38) is performed using an implicit θ-scheme with for
365 both advection and dispersion, which leads to:

366
$$\frac{1}{\Delta t}[A]\begin{bmatrix}\tilde{c}\\ \tilde{c}\\ \tilde{c}\end{bmatrix}_E + \theta\left[M^2+N^2\right]\begin{bmatrix}\tilde{c}\\ \tilde{c}\\ \tilde{c}\end{bmatrix}_E + \theta\left[M^4+N^4\right]\begin{bmatrix}\tilde{c}\\ \tilde{c}\\ \tilde{c}\end{bmatrix}_{E'}^{n+1} + \theta\left[M^4+N^4\right]\begin{bmatrix}\tilde{c}\\ \tilde{c}\\ \tilde{c}\end{bmatrix}_E$$
$$= \frac{1}{\Delta t}[A]\begin{bmatrix}\tilde{c}\\ \tilde{c}\\ \tilde{c}\end{bmatrix}_E - (1-\theta)\left[M^2+N^2\right]\begin{bmatrix}\tilde{c}\\ \tilde{c}\\ \tilde{c}\end{bmatrix}_E$$

367 (39)

368 Notice that the developed DG method comes down to the upwind finite volume scheme on the
369 lumping regions if the second and the third equations of system (39) are removed. In all the
370 simulations reported hereafter, the value of θ is fixed to 1/2, which corresponds to the Crank-
371 Nicolson scheme.

4. Numerical Experiments

The new DG-MFE formulation is first compared with an analytical solution. It is then used to simulate: (*i*) solute transport in the case of surface contamination with a total flux boundary condition, and (*ii*) in the case of a steady-state transport problem between an injection/extraction well pair.

4.1 Comparison against the analytical solution

The analytical solution was developed by [43] for a simplified 2D transport problem (Fig. 3) and was employed by [14] and [15] for the verification of numerical codes. The domain is a rectangle of dimension $(0-100m)\times(0-40m)$ with a uniform flow from left to right (Fig. 3).

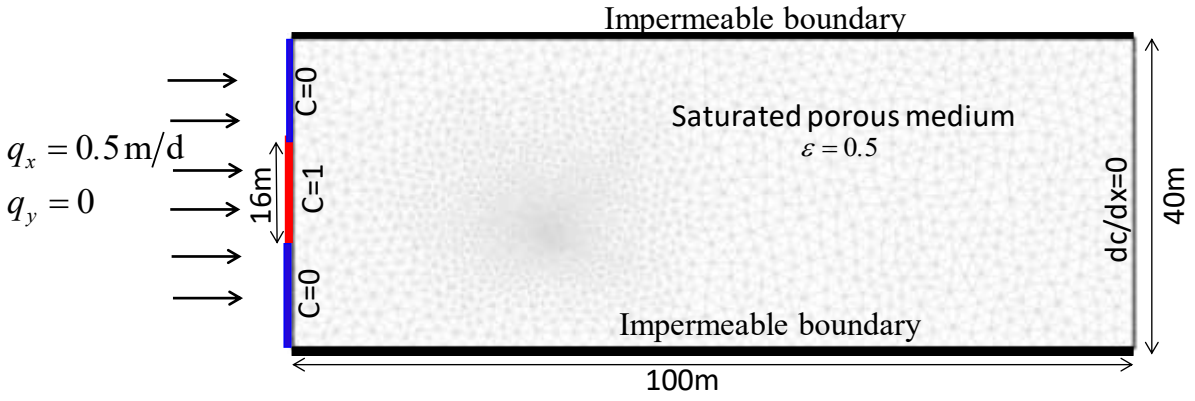

Fig.3. Description of the problem of transport in a 2D domain with a uniform flow.

A Dirichlet boundary condition is prescribed for the concentration at the inflow boundary with:

$$C = \begin{cases} 0 & \text{for } 0 \le y < 12 \\ 1\,g/l & \text{for } 12 \le y \le 28 \\ 0 & \text{for } 28 < y \le 40 \end{cases} \tag{40}$$

The right side is an outflow boundary (null diffusive flux) and the lateral (no flow) boundaries are impermeable. The fluid flow is uniform over the domain with a constant horizontal velocity $q_x = 0.5$ m/day imposed at the left boundary and a uniform porosity $\varepsilon = 0.5$. The simulation

389 is performed for a final simulation time T = 30 days.

390 The analytical solution to this test case for an infinite domain is given by [43]:

391 $$C_{analy}(x,y,t) = \frac{x}{(16\pi\alpha_L)^{1/2}} \int_0^T \tau^{-3/2} \left\{ erf\left[\frac{y-12}{(4\alpha_T\tau)^{1/2}} \right] + erf\left[\frac{28-y}{(4\alpha_T\tau)^{1/2}} \right] \right\} exp\left[-\frac{(x-\tau)^2}{4\alpha_L\tau} \right] d\tau$$

392 (41)

393 with $erf(x) = \frac{2}{\sqrt{\pi}} \int_0^x exp(-\tau^2)\, d\tau$.

394 The domain is discretized with an unstructured triangular mesh formed by 4000 elements.
395 Although, the test case involves a uniform velocity field, a local refinement is performed around
396 the point (30m, 15m) to obtain a highly unstructured mesh with significant differences in the
397 distribution of the Courant and grid Peclet numbers inside the domain. Furthermore, we located
398 the refinement in the expected transition zone, where the gradient of the concentration is high,
399 in order to detect the eventual impact of the mesh on the solution.

400 The comparison between the analytical and numerical solutions is performed for three test
401 cases, from highly convective to highly dispersive scenarios (Table 1), characterized by their
402 Peclet number defined for the investigated horizontal flow as:

403 $$Pe_{L,T} = \frac{\sum_j \left| Q_j^E \right|}{2\alpha_{L,T} \left\| \boldsymbol{q} \right\|} \quad (42)$$

404 where $Pe_{L,T}$ is the grid Peclet number in either the longitudinal (L) or the transverse (T) direction
405 and $\|\boldsymbol{q}\|$ is the velocity norm. The different values of dispersivities (α) are given in Table 1
406 with the range of Peclet numbers (irregular grid).

407

Test case	α_L (m)	α_T (m)	$< Pe_L >$ (-)	σ_{Pe_L} (-)	$< Pe_T >$ (-)	σ_{Pe_T} (-)
TC1_A	0.05	0.01	27.3	13.3	136.3	66.7
TC1_AD	0.5	0.2	2.73	1.33	6.81	3.33
TC1_D	5.0	1.0	0.273	0.133	1.36	0.66

Table 1. Dispersivities and Peclet numbers (average and standard deviation) for the different test cases (_A stands for advective dominant, _AD for advective-dispersive, and _D for dispersive dominant transport).

The three test cases are simulated using a large time step of $\Delta t = 1\,\mathrm{d}$. It is worth noting that the new developed scheme is not constrained by the CFL condition since we use an implicit scheme. This feature departs from the classical approach, based on operator and time splitting (Eqs (5)-(6)) with an explicit time discretization for the advection operator and an implicit discretization for dispersion [14, 27, 35, 36 and 37]. For stability reasons, the explicit time discretization requires the strict respect of the CFL condition $\left(CFL \le 0.5\right)$, with a CFL defined by [44]):

$$CFL = \frac{\sum_j \left|Q_j^E\right|}{2\left|E\right|}\Delta t \tag{43}$$

where $\left|E\right|$ is the area of element *E*.

Thus, for the classical approach with an explicit time discretization, the time step should be less than a critical value $\Delta t_c = 0.04\,\mathrm{d}$ corresponding to $\left(CFL = 0.5\right)$. This critical time step corresponds to the smallest element in the domain since the velocity field is uniform. The time step with the new model is therefore 25 times greater than that allowed by the explicit scheme. This gain can be much more important if the CFL constraint is more severe, as for instance, in the presence of an injection or a pumping well, where the region around the well is usually characterized by mesh refinement and high velocities.

Fig. 4 depicts the numerical and analytical concentration profiles at x = 20m and y = 20m for the three test cases. Sharp longitudinal and transverse concentration profiles are observed for the advection dominated scenario (TC1_A) whereas, widely spread concentration fronts are obtained in the dispersion dominated test scenario (TC1_D).

The results of the three test cases show a very good agreement between the analytical and the numerical solutions. These results validate the new edge-centered DG-MFE model as able to accurately simulate solute transport in a wide panel of settings from advection dominated to dispersion dominated transport.

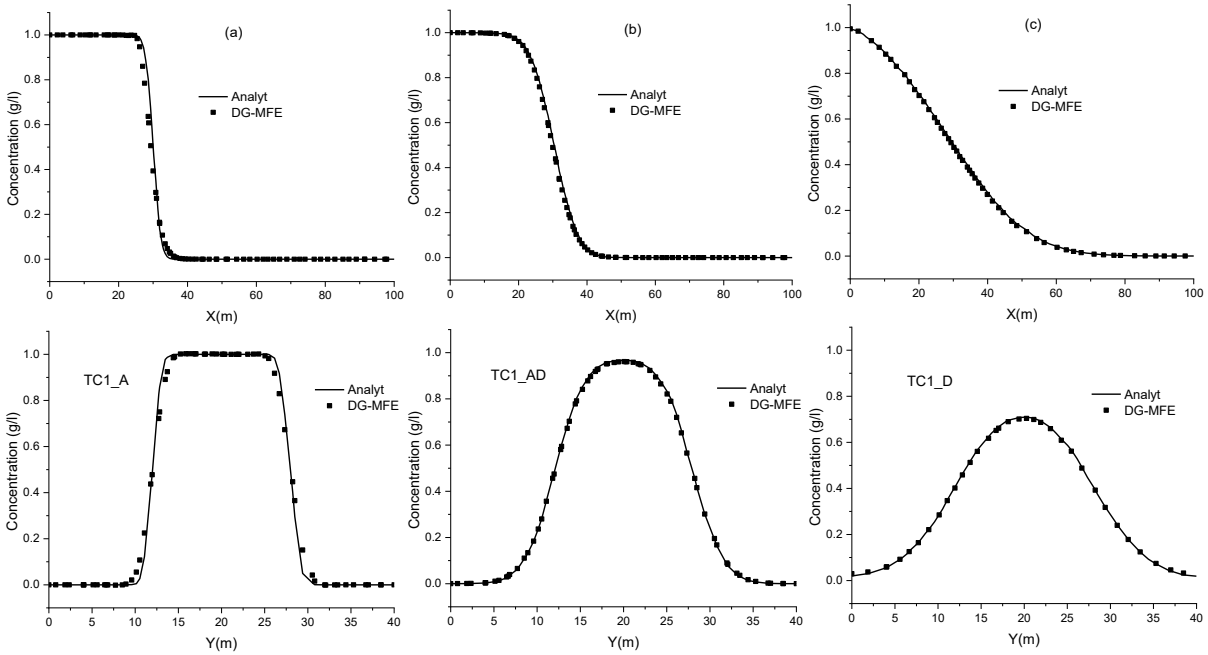

Fig. 4: Analytical and numerical concentrations for longitudinal profiles at x = 20m and transversal profiles at y = 20m for the three test cases.

To investigate the order of convergence of the edge-centered DG-MFE formulation, the advective-dispersive test problem **TC1_AD** is simulated using different mesh sizes. We start with a uniform unstructured mesh formed by 1004 triangles and fix the time step to a small value of $\Delta t = 0.01d$ for all simulations. In each level of refinement, each triangle is subdivided into four similar triangles, by joining its three mid-edges of the initial triangle. The L_2 error $\left(L_2 Er\right)$ is then calculated at the simulation time $T_f = 20d$ for the different meshes. The runs are performed on a single computer with an Intel Xeon E-2246G processor and 32 GB memory. The results of the simulations, plotted in Fig. 5, show an average order of convergence in space of 1.63 for the investigated **TC1_AD** test problem.

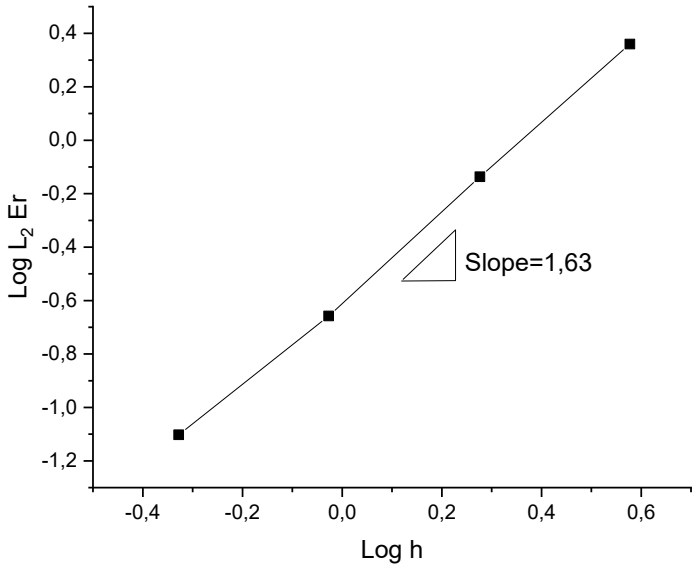

Fig. 5: Convergence in space of the edge-centered DG-MFE formulation for the **TC1_AD** test problem.

To investigate the convergence in time, the **TC1_AD** test problem is simulated using a fine spatial discretization formed by 16064 elements and different time steps for $\theta = 1$ (full-implicit) and $\theta = 0.5$ (Crank-Nicolson) schemes. Results in Fig. 6 show that both schemes yield an order of convergence around 1. Nevertheless, the Crank-Nicolson scheme is much more accurate than the implicit scheme. For a given space and time discretization, the L_2 error with the Crank-Nicolson scheme is on average 2.3 lower than that of the implicit scheme (Table2).

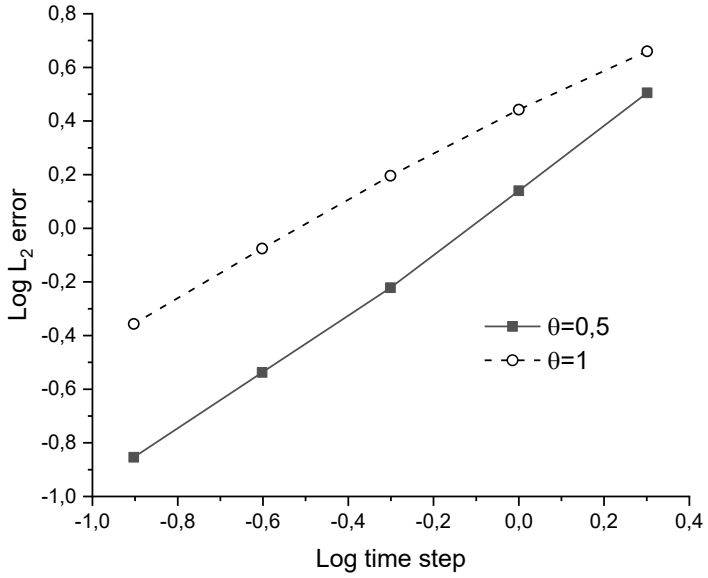

459

460 **Fig. 6**: Convergence in time of the edge-centered DG-MFE formulation with $\theta = 1$ (implicit)

461 and $\theta = 0.5$ (Crank-Nicolson) schemes for **TC1_AD** test problem.

462

Δt	$L_2^{\theta=0.5} Er$	$L_2^{\theta=1} Er$	$L_2^{\theta=1} Er / L_2^{\theta=0.5} Er$	CPU time (s)
2	3.2	4.57	1.43	0.7
1	1.38	2.77	2.0	1.0
0.5	0.6	1.57	2.6	1.65
0.25	0.29	0.84	2.9	3.0
0.125	0.14	0.44	2.6	5.62

463 Table 2: Convergence in time of the edge-centered DG-MFE formulation for **TC1_AD** test

464 problem.

465 *4.2 Transport simulation with total flux boundary condition*

466 The proposed edge-centered DG-MFE formulation is well adapted to simulate transport

467 problems involving total flux boundary conditions since advection and dispersion are treated in

468 a single system. A 2D transport problem is simulated with a total flux boundary condition over

the same domain as that of the previous test case TC1.

The boundary conditions for flow and transport are described in Fig. 7. The hydraulic conductivity of the porous material is $K = 10\,m/d$. The prescribed total (advection and dispersion) lateral solute flux is $q_t = 1\,g/\left(m^2 d\right)$ and the injected water flux is $q_w = 0.2m/d$.

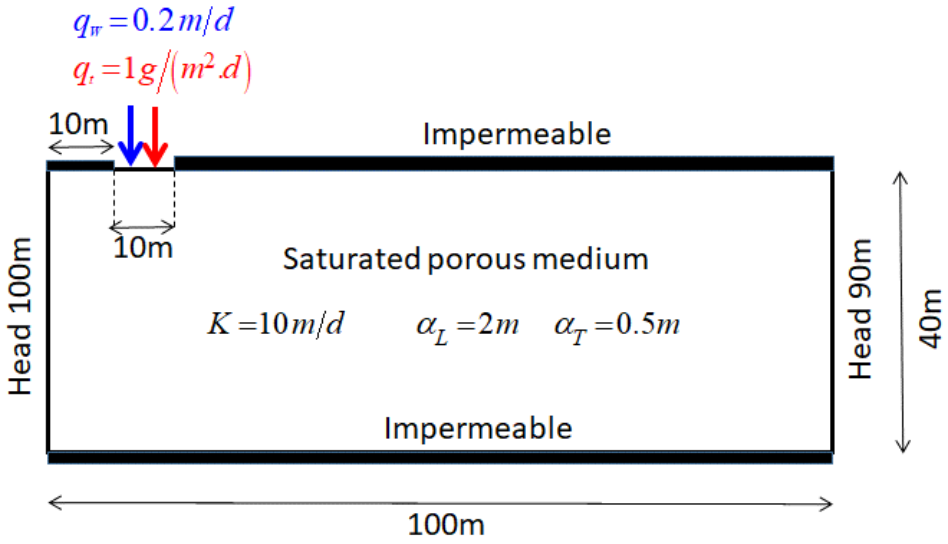

Fig. 7: Description of the 2D transport problem with lateral injection as a total flux boundary condition.

To obtain the velocity field, we first solve the following steady-state Darcy's flow:

$$\begin{cases} \nabla . \boldsymbol{q} = q_S \\ \boldsymbol{q} = -\boldsymbol{K} \nabla H \end{cases} \tag{44}$$

where $\boldsymbol{q}$ is the Darcy velocity [LT^{-1}], q_S the source/sink term [T^{-1}], H the water head [L], and $\boldsymbol{K}$ the hydraulic conductivity tensor [LT^{-1}].

The flow system is solved with the mixed finite element method ([4]) under the corresponding Dirichlet (prescribed head) and Neumann (prescribed flux) boundary conditions reported in Fig. 7.

Since there is no analytical solution for the investigated problem, the transport solution of the new DG-MFE scheme is compared to the solution obtained with COMSOL multiphysics

485 software v. 6.1. (www.comsol.com) which is based on the standard Galerkin Finite Element
486 (GFE) method. Two test cases are investigated: TC2_A (advection dominated) with
487 $\alpha_L = 0.02m$ and $\alpha_T = 0.005m$, and TC2_D (dispersion dominated) with $\alpha_L = 2m$ and
488 $\alpha_T = 0.5m$.

489 The concentration distributions at t = 60 days for both cases are plotted in Fig. 8. For the case
490 TC2_A, the solute remains near the injected lateral boundary of the domain, whereas, for
491 TC2_D, solute is more spread over the domain because of large transverse dispersion. Results
492 in Fig. 6 show a very good agreement between DG-MFE and GFE solutions in the case of high
493 dispersion. When advection is dominant, a less satisfactory agreement is observed between the
494 two solutions. The DG-MFE solution shows a sharp solute interface (see the tight iso-
495 concentration lines in Fig. 8), while the interface is smoother with the GFE scheme due to
496 numerical diffusion. Notice that in both test cases and for both DG-MFE and FE models, the
497 concentration at the injection region is not fixed but calculated during the simulation to fulfill
498 the total (advection + dispersion) flux conditions. For TC2_A, the concentration at the injection
499 region reaches 4.96 g/l. For TC2_D, it is lower, due to dispersion (C= 2.8 g/l).

500

501

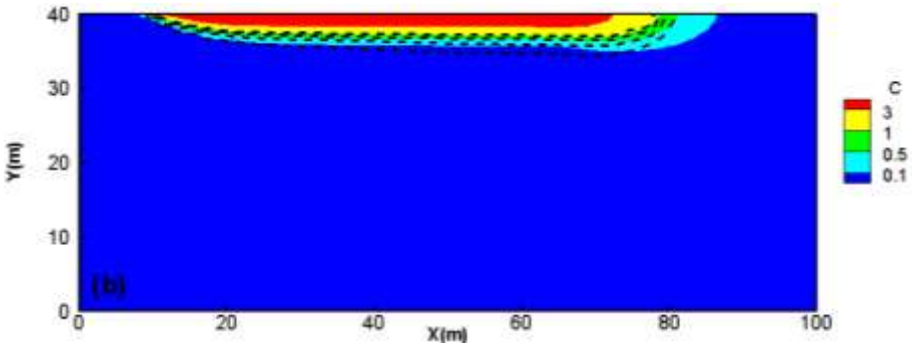

502

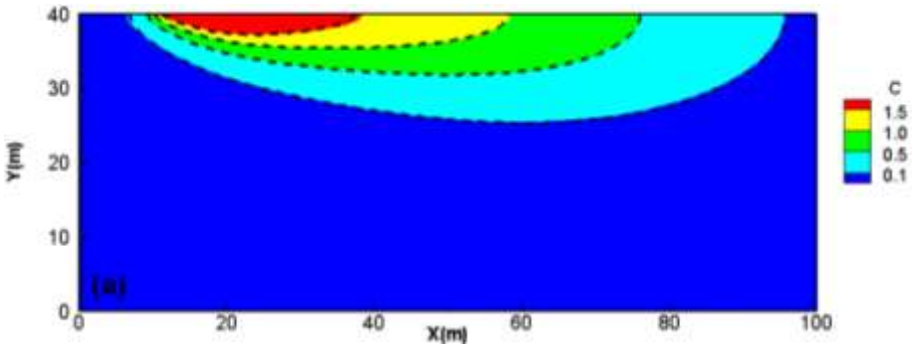

Fig. 8. Concentration distributions for transport with a prescribed total flux boundary condition. Results of FE (color map) and DG-MFE (dashed lines) models for TC2_A (top) and TC2_D (bottom).

For a deeper comparison between the two models, we plot in Fig. 9 the evolution of concentrations near the injection region, at the observation point located in $(x = 20m, y = 40m)$. There is a very good agreement between the GFE and DG-MFE breakthrough curves for the case TC2_D with high dispersion. For TC2_A, the breakthrough curve from the GFE model shows unphysical oscillations near the sharp concentration front, those being absent from the DG-MFE results. Notably, by neglecting dispersion and assuming a total flux as that of advection only, the concentration at the injection region should be $\overline{C} = \frac{q_t}{q_W} = 5\,g/l$. When dispersion is present, the concentration C should always be smaller than $\overline{C}$ (red line in Fig. 9). The asymptotic value reached by the DG-MFE model at the observation point is 4.96 g/l (Fig. 9), whereas the GFE model shows an asymptotic concentration value of 5.12 g/l which is unphysical since it exceeds $\overline{C}$. These results highlight the very good accuracy of the DG-MFE model for advection-dominated transport problems with total flux boundary conditions.

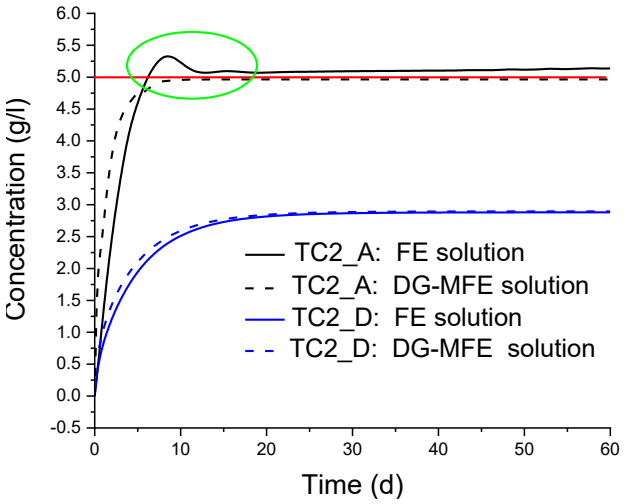

521

522 **Fig. 9.** Concentration evolution at $(20m, 40m)$ with the GFE and DG-MFE schemes.

523

524 *4.3 Steady-state transport simulation of an injection/extraction well pair problem*

525 This test problem considers the contamination of a 2D confined homogeneous domain where
526 the flow field is induced by a pair of extraction (sink) and injection (source) wells in an initially
527 uniform sweeping flow over the whole modeled area. The domain has a square shape of
528 $100m \times 100m$ (Fig. 10) with initial (before the wells are active) uniform flow, occurring from
529 the left side, with head fixed to $H_L = 102m$ and inlet concentration fixed to $C_L = 0$, toward the
530 right side, with head fixed to $H_R = 100m$ and a null diffusive flux for transport. The hydraulic
531 conductivity is $2m/d$ and the longitudinal and transverse dispersivities are $\alpha_L = 2m$ and
532 $\alpha_T = 0.5m$, respectively. The lag distance between the sink and source terms is 18 m. Solute is
533 injected at a fixed rate of $3m^2/d$ at the location ($x = 41m$, $y = 50m$) and extracted at ($x = 59m$,
534 $y = 50m$) where the hydraulic head is prescribed at $H_{extract} = 98m$. An unstructured triangular
535 mesh with local mesh refinement in the vicinity of the injection and extraction wells (Fig. 10)
536 is used for both flow and transport simulations.
537 The flow problem is solved by the MFE method ([4]). The hydraulic head distribution and path
538 lines representing fluid particles trajectories are drawn in Fig. 11, showing that the extraction

well captures almost all the water from the injection and a fraction of water coming from the left boundary. Although the head at the sink $\left(H_{extract}=98m\right)$ is less than that of the right boundary $\left(H_R=100m\right)$, no flow occurs from the right boundary toward the extraction well.

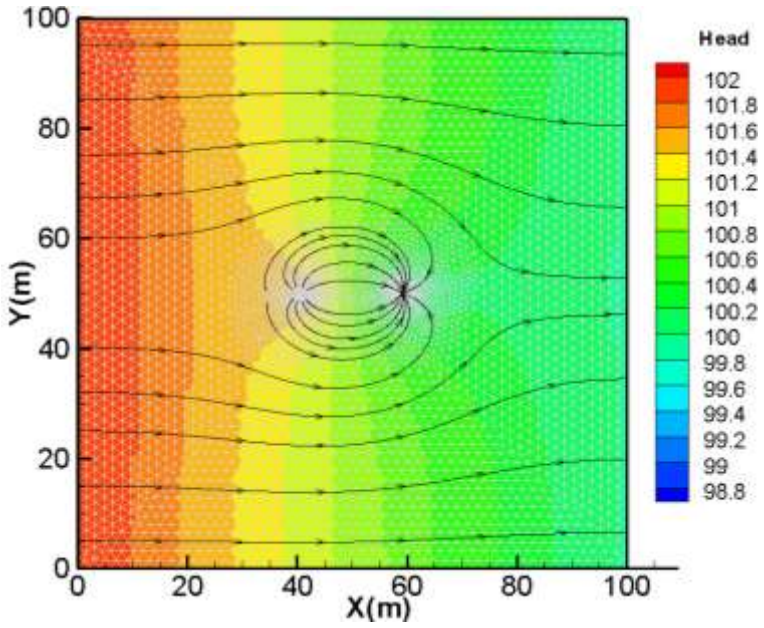

Fig. 10. Results of the flow simulation for the injection/extraction well pair problem.

In this example, we are interested in the distribution of a solute invading the system from a continuous injection to a distant continuous extraction, the whole resulting in a steady-state solute plume. The direct steady-state simulation is not possible with the classical DG-MFE formulation based on operator and time splitting. In addition, the long-term transient simulation of transport until reaching the steady-state solution is hardly affordable with classical DG-MFE. Usually, the classical formulation is associated with an explicit time discretization of the advection operator which requires the strict respect of the CFL criterion. In the present test case, the high magnitude of velocities and the small element size in the vicinity of the injection and extraction wells, would imply a time step of $\Delta t \le 1.310^{-3} d$ to respect the CFL criterion. Given that the steady-state regime (when the total mass in the system becomes constant) is reached at approximately $T=5000d$, the classical approach with an explicit scheme would requires

556 4×10^6 time steps to reach the steady-state regime.

557 The new DG-MFE numerical scheme can be employed to obtain the steady-state solution in a
558 single step only requiring 0.3s of CPU time. Fig. 11 compares the solution from the steady-state
559 calculation and that of a transient simulation (also performed by solving Eq. (39)) using 5000
560 time steps of $\Delta t = 1d$. In the latter, the whole simulation needs for approximately 87s of CPU
561 time.

562 A very good agreement is observed between the steady-state and the "transient" solutions (Fig.
563 11), while the steady-state calculation is approximately 300 times faster than the transient
564 calculation. Fig. 11 also reports on the steady-state solution obtained with a fully upwind MFE
565 method (described in [15]) in which the MFE is complemented by an upwind scheme for
566 advection to avoid unphysical oscillations due to the hyperbolic nature of the operator. As
567 expected, the steady-state solution from the fully upwind MFE scheme shows (dashed iso-
568 concentration lines in Fig. 11) large numerical diffusion, which renders it less accurate than the
569 DG-MFE solution.

570 These results point out the accuracy of the new DG-MFE scheme compared with the fully
571 upwind MFE solution; they also highlight how efficient the new scheme can be for single-step
572 steady-state simulations (and also here, accurate for implicit transient simulations even with
573 large time steps).

574

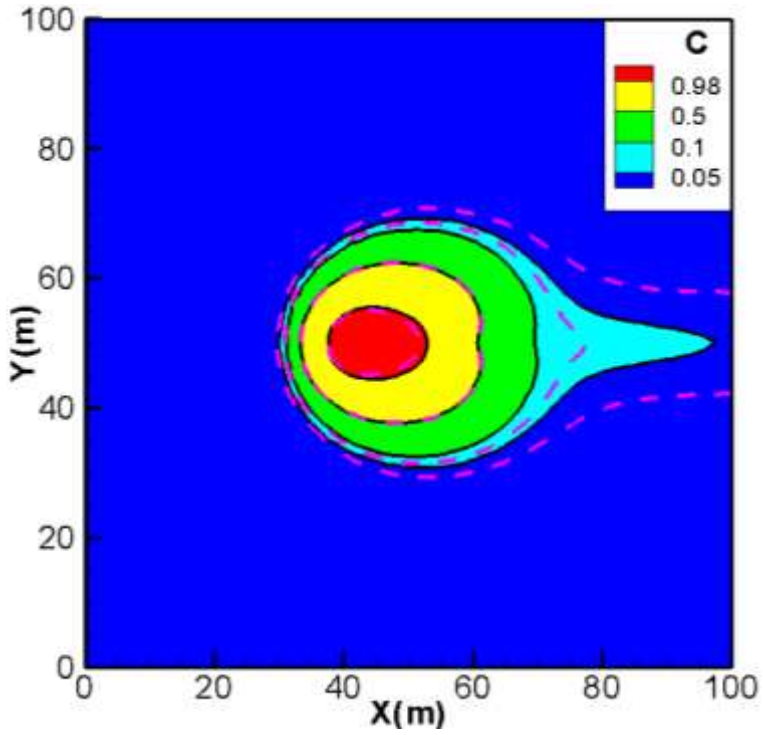

Fig. 11: Results of transport simulations for the injection/extraction pair problem. Steady-state DG-MFE simulation (black lines), transient DG-MFE simulation using 5000 time steps of 1 day (color maps), and steady-state upwind-MFE simulation (purple dashed lines).

5. Conclusions

We propose in this work a new DG-MFE scheme to solve the advection-dispersion equation. The DG method is developed over the lumping regions associated with the mesh edges and is combined with the lumped MFE method. The DOFs of DG are the mean concentration on the lumping region complemented by the deviation of the concentration in each space direction. This allows for obtaining a single system of equations with common DOFs (edge concentration) for both advection and dispersion discrete operators. The temporal discretization is based on the Crank–Nicolson method for both advection and dispersion.

The accuracy of the new DG-MFE formulation was investigated using three types of problems involving a full dispersion tensor. The first test problem highlights the accuracy of the DG-

MFE model by comparing the calculations with analytical solutions for highly advective transport problems, moderately and highly dispersive problems. The results of the new DG-MFE model showed very good agreements with the analytical solution for all the investigated scenarios. The second test case handled a transport problem with a total flux boundary condition. For this problem, the DG-MFE solution was compared to the GFE solution obtained with Comsol software in the cases of both advection-dominated and dispersion-dominated transports. The results showed a very good agreement between the GFE and DG-MFE concentration curves in the case of high dispersion. In the case of high advection, the concentration profile with GFE concealed unphysical oscillations and reached anomalous asymptotic concentration values. These drawbacks are avoided with the new DG-MFE model. Finally, the DG-MFE model was used for the steady-state transport simulation with sink and source terms. A very good agreement was obtained between the steady-state and the long-term transient simulation results, while, the steady-state calculation required approximately 300 times less CPU time than the transient calculation. The steady-state problem was also simulated with the fully upwind MFE method which resulted in a solution with large numerical diffusion. These results highlight the efficiency of the new DG-MFE model for steady-state transport simulations that cannot be performed with the classical approach. They also point out the accuracy of the obtained solution as compared to the fully upwind MFE solution.

The 2D formulation is quite generic and can be extended to 3D tetrahedral elements without too much complicated numerical developments. These numerical investigations are under progress.

CRediT authorship contribution statement

Anis Younes: Conceptualization, Methodology, Software, Supervision, Validation, Writing – original draft, Writing – review & editing. Frederick Delay: Validation, Writing – original draft, Writing – review & editing. Philippe Ackerer: Methodology, Validation, Writing – review & editing.

Declaration of competing interest

We declare that we have no known competing financial interests or personal relationships that could have influenced the work reported in this paper.

Data availability

The FORTAN90 code is available on request.

Acknowledgements

This work was supported by the French National Center of Research (CNRS) and Strasbourg University.

References

[1] Raviart, P. A., Thomas, J. M., A mixed finite element method for 2-nd order elliptic problems, in: Mathematical Aspects of Finite Element Methods, Berlin, Heidelberg, (1977), 292–315.

[2] Chavent, G., Jaffré, J., Mathematical models and finite elements for reservoir simulation: single phase, multiphase, and multicomponent flows through porous media, North-Holland ; Sole distributors for the U.S.A. and Canada, Elsevier Science Pub. Co, Amsterdam ; New York : New York, N.Y., U.S.A, (1986), 376 p.

[3] Brezzi, F., Fortin, M. (Eds.), Mixed and Hybrid Finite Element Methods, Springer New York, New York, NY (1991), https://doi.org/10.1007/978-1-4612-3172-1.

[4] Younes, A., Ackerer, P., Delay, F., Mixed finite elements for solving 2-D diffusion-type equations, Rev. Geophys., 48, (2010), RG1004, https://doi.org/10.1029/2008RG000277.

[5] Mosé, R., P. Siegel, Ph. Ackerer, G. Chavent, Application of the mixed hybrid finite element approximation in a groundwater flow model: luxury or necessity? Water Resour. Res., 30, (1994), 3001-3012. https://doi.org/10.1029/94WR01786.

[6] Durlofsky, L. J., Accuracy of mixed and control volume finite element approximations to Darcy velocity and related quantities, Water Resour. Res. 30, (1994), 965-973. https://doi.org/10.1029/94WR00061.

[7] Hoteit, H., A. Firoozabadi, Modeling of multicomponent diffusions and natural convection in unfractured and fractured media by discontinuous Galerkin and mixed methods: Modeling of multicomponent diffusions and natural convection, Int J Numer Methods Eng. 114 (2018) 535–556. https://doi.org/10.1002/nme.5753.

[8] Fraeijis de Veubeke B.M., Hogge M.A., Dual analysis for heat conduction problems by finite elements. Int. J. Numer. Meth. Eng., 5, (1972), 65-82.

[9] Chavent, G., Roberts, J. E., A unified physical presentation of mixed, mixed-hybrid finite elements and standard finite difference approximations for the determination of velocities in waterflow problems, 14, (1991),329–348, https://doi.org/10.1016/0309-1708(91)90020-O.

[10] Traverso, L., Phillips, T. N., Yang, Y., Mixed finite element methods for groundwater flow in heterogeneous aquifers, Computers & Fluids, 88, (2013), 60–80, https://doi.org/10.1016/j.compfluid.2013.08.018.

[11] Younes, A., Ackerer, P., Lehmann, F., A new mass lumping scheme for the mixed hybrid finite element method, International Journal for Numerical Methods in Engeneering, 67, (2006), 89–107, https://doi.org/10.1002/nme.1628.

[12] Hoteit, H., Mosé, R., Philippe, B., Ackerer, P., Erhel, J., The maximum principle violations of the mixed-hybrid finite-element method applied to diffusion equations: Mixed-hybrid finite element method, 55, (2002), 1373–1390, https://doi.org/10.1002/nme.531.

[13] Mazzia, A., An analysis of monotonicity conditions in the mixed hybrid finite element method on unstructured triangulations, 76, (2008), 351–375, https://doi.org/10.1002/nme.2330.

[14] Siegel, P., Mosé, R., Ackerer, P., and Jaffré, J., Solution of the Advection Diffusion Equation using a combination of Discontinuous and Mixed Finite Elements, Int. J. Numer. Meth. Fluids, 24: 595-613, (1997), https://doi.org/10.1002/(SICI)1097-0363(19970330)24:6<595::AID-FLD512>3.0.CO;2-I.

[15] Younes, A., Hoteit H., Helmig R., Fahs M., A robust upwind mixed hybrid finite element method for transport in variably saturated porous media, Hydrol. Earth

680 Syst. Sci., 26, (2022), 5227–5239, https://doi.org/10.5194/hess-26-5227-2022.
681 [16] Cockburn B., Hou S., Shu C.-W., TVB Runge-Kutta local projection discontinuous
682 Galerkin finite element method for conservation laws III: One-dimensional
683 systems, J. Comput. Phys. 84 (1989), 90. https://doi.org/10.1016/0021-
684 9991(89)90183-6
685 [17] Cockburn B., Shu C.-W., The Runge-Kutta local projection P1-discontinuous Galerkin
686 method for scalar conservation laws, M2 AN 25 (1991), 337.
687 [18] Cockburn B., Shu C.-W., The Runge-Kutta discontinuous Galerkin method for
688 conservation laws V: Multidimensional systems, J. Comput. Phys. 141 (1998),
689 199-224. https://doi.org/10.1006/jcph.1998.5892
690 [19] Oden J. T., Babuska I., Baumann C. E., A discontinuous hp finite element method for
691 diffusion problems, Journal of Computational Physics 146 (1998), 491-519.
692 https://doi.org/10.1006/jcph.1998.6032
693 [20] Cockburn B., Shu C.-W., The local discontinuous Galerkin finite element method for
694 convection-diffusion systems, SIAM J. Numer. Anal. 35 (1998), 2440-2463.
695 https://doi.org/10.1137/S0036142997316712
696 [21] Rivière B., Wheeler M. F., Girault V., A priori error estimates for finite element
697 methods based on discontinuous approximation spaces for elliptic problem, SIAM
698 Journal on Numerical Analysis 39, 3, (2001), 902-931.
699 doi:10.1137/S003614290037174X
700 [22] Arnold D. N., Brezzi F., Cockburn B., Marini L. D., Unified analysis of discontinuous
701 Galerkin methods for elliptic problems, SIAM J. Numer. Anal. 39, 5, (2002),
702 1749-1779. https://doi.org/10.1137/S0036142901384162
703 [23] Hoteit H., Ackerer Ph., Mosé R., Erhel J., Philippe B., New two-dimensional slope
704 limiters for discontinuous Galerkin methods on arbitrary meshes, Int. J. Numer.

Methods Eng. 61 (2004) 2566-2593. https://doi.org/10.1002/nme.1172

[24] Burbeau A., Sagaut P., Bruneau C. H., A Problem-Independent Limiter for High-Order Runge-Kutta Discontinuous Galerkin Methods, J. Comput. Phys. 169 (2001) 111-150. https://doi.org/10.1006/jcph.2001.6718

[25] Younes, A., Fahs, M., Ackerer, P., An efficient geometric approach to solve the slope limiting problem with the discontinuous Galerkin method on unstructured triangles. International Journal for Numerical Methods in Biomedical Engineering, 26(12), (2010), 1824-1835. https://doi.org/10.1002/cnm.1268

[26] Younes, A., Ackerer P., Solving the advection-dispersion equation with discontinuous Galerkin and multipoint flux approximation methods on unstructured meshes, Int. J. Numer. Methods Fluids,58(6), (2008), 687–708, doi:10.1002/fld.1783.

[27] Ackerer, P., Younes, A., Mose, R., Modeling Variable Density Flow and Solute Transport in Porous Medium: 1. Numerical Model and Verification. Transport in Porous Media 35, (1999), 345–373, https://doi.org/10.1023/A:1006564309167.

[28] Moortgat, J., Firoozabadi A., Mixed-hybrid and vertex-discontinuous-Galerkin finite element modeling of multiphase compositional flow on 3d unstructured grids, J. Comput. Phys., 315, (2016), 476–500, doi:10.1016/j.jcp.2016.03.054.

[29] Younes, A., Ph. Ackerer, G. Chavent (2004), From mixed finite elements to finite volumes for elliptic PDE in 2 and 3 dimensions. Int. J. Num. Meth. Eng., 59, 365–388.

[30] Younes, A., V. Fontaine (2008), Hybrid and multi-point formulations of the lowest-order mixed methods for Darcy's flow on triangles. Int. J. Num. Meth. Fluids, 58, 9, pp 1041-1062.

[31] Wheeler, M.F., I. Yotov (2006), A multi-point flux mixed finite element method. SIAM J. Numer. Anal. 44, 2082–2106.

730 [32] Kirby R. A posteriori error estimates and local time-stepping for flow and transport
731 problems in porous media. Ph.D. Thesis, University of Texas at Austin, 2000.
732 [33] Dawson, C.N., Wheeler M.F., Time-splitting methods for advection–diffusion-reaction
733 equations arising in solute transport, in: ICIAM 91, Washington, DC, 1991
734 (SIAM, Philadelphia, PA, 1992), pp. 71–82.
735 [34] Hoteit, H., Firoozabadi A., Multicomponent fluid flow by discontinuous Galerkin and
736 mixed methods in unfractured and fractured media: multicomponent fluid flow in
737 fractured media, Water Resour. Res. 41 (2005).
738 https://doi.org/10.1029/2005WR004339.
739 [35] A. Mazzia, L. Bergamaschi, M. Putti, A time-splitting technique for advection–
740 dispersion equation in groundwater, J. Comput. Phys. 157 (1) (2000) 181–198.
741 [36] A. Mazzia, L. Bergamaschi, C.N. Dawson, M. Putti, Godunov mixed methods on
742 triangular grids for advection–dispersion equations, Comput. Geosci. 6 (2) (2002)
743 123–139.
744 [37] A. Mazzia, M. Putti, Mixed-finite element and finite volume discretization for heavy
745 brine solutions in groundwater, J. Comput. Appl. Math. 147 (1) (2002) 191–213.
746 [38] Mazzia, A.; Manzini, G.; Putti, M. 2011: Bad behavior of Godunov mixed methods for
747 strongly anisotropic advection—dispersion equations Journal of Computational
748 Physics 230(23): 8410-8426
749 [39] Mazzia, A.; G.; Putti, M. 2005, High order Godunov mixed methods on tetrahedral
750 meshes for density driven flow simulations in porous media. Journal of
751 Computational Physics 208 (2005) 154-174.
752 [40] El Soueidy, Ch.P., Younes, A., Ackerer, P.: Solving the advection-diffusion equation
753 on unstructured meshes with discontinuous/mixed finite elements and a local time
754 stepping procedure. Int. J. Numer. Methods Eng. 79, 1068–1093 (2009)

[41] Belfort, B., Ramasomanana, F., Younes, A., and Lehmann, F.: An Efficient Lumped Mixed Hybrid Finite Element Formulation for Variably Saturated Groundwater Flow, 8, 352–362, https://doi.org/10.2136/vzj2008.0108, 2009.

[42] Koohbor, B., Fahs, M., Hoteit, H., Doummar, J., Younes, A., and Belfort, B.: An advanced discrete fracture model for variably saturated flow in fractured porous media, 140, 103602, https://doi.org/10.1016/j.advwatres.2020.10hy3602, 2020.

[43] Leij, F. J., Dane, J. H., Analytical solutions of the one-dimensional advection equation and two- or three-dimensional dispersion equation, 26, (1990), 1475–1482, https://doi.org/10.1029/WR026i007p01475.

[44] Putti, M., Yeh, W.W.-G., Mulder, W.A., A triangular finite volume approach with high-resolution upwind terms for the solution of groundwater transport equations, Water Resources Res., 26, (1990), 2865-2880, https://doi.org/10.1029/WR026i012p02865.